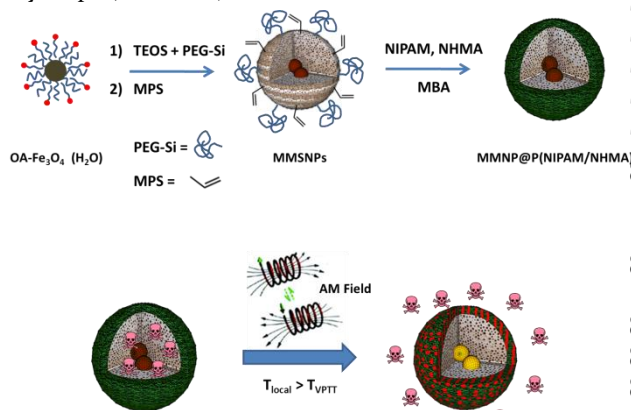


gies commonly required for heating the environment, thus overcoming the blood-mediated thermal dissipation. For this goal, the mesoporous silica surface was coated with an engineered thermosensitive random copolymer which exhibits a linear (soluble) to globular (insoluble) transition at 40-43°C. Therefore in physiological temperature, the polymer chains are extended and soluble, blocking the release, while above the transition temperature the polymer shrinks, allowing the cargo release. The archstone for this performance is the hot spots formed by the superparamagnetic iron oxide nanoparticles (SPION) that are embedded in the mesoporous silica matrix, in response to an alternate magnetic field. This hot spot effect is shown to be capable to reach the polymer coating that blocks the mesopores, thus provoking the shrinkage of the polymer network and the release of its cargo.

The colloidal stability of nanocarriers is crucial for biomedical applications, especially in the case of intravenous administration²¹. Mesoporous silica nanoparticles have been widely studied as drug delivery vehicles but they often suffer from aggregation in the bloodstream, that could be solved by polymer attachment on the silica surface²². Coating of nanoparticles with poly(ethylene glycol) or other hydrophilic polymers is known to improve their colloidal stability in physiological conditions and increase their circulation times²³. Therefore, we have developed a synthetic procedure of magnetic mesoporous silica nanoparticles based on the following key steps (Scheme 1).



Scheme 1. Synthesis path of MMSN@P(NIPAM/NHMA) device.

EXPERIMENTAL SECTION

Reagents. All chemicals were used without further purification. Tetraethyl orthosilicate (TEOS, 98%), n-Cetyltrimethylammonium bromide (CTAB, 99%), [Tris(trimethylsilyloxy)silyl]propyl methacrylate (TMSPPMA, 98%), N-Isopropylacrylamide (NIPAM, ≥99%), N-(Hydroxymethyl)acrylamide solution (NHMA, 48 wt. % in H₂O), N,N'-Methylenebis(acrylamide) (MBA, 99%) Oleic acid (OA, ≥99%), 4,4'-Azobis(4-cyanovaleric acid) (ABCVA, ≥98.0%), fluorescein sodium salt, iron (II) chloride tetrahydrate (FeCl₂·4H₂O, 99%) and iron (III) chloride hexahydrate (FeCl₃·6H₂O, >99%) were obtained from Sigma Aldrich. [Hydroxy(polyethyleneoxy)propyl] tri-

ethoxysilane, (PEG-Si, MW = 575-750 g/mol, 50 % in ethanol) was purchased from Gelest. Ammonium nitrate (NH₄NO₃, 99.9%), ammonium hydroxide (NH₄OH, 28-30 wt % as NH₃), chloroform (CHCl₃, 99.8%), sodium hydroxide (NaOH, ≥98%), absolute ethanol were purchased from Panreac. Ultrapure water was generated using a Millipore Milli-Q system with a Milli-pak filter of 0.22 μm pore size and used for all the preparation of aqueous solutions.

Characterization Techniques. Fourier transform infrared spectroscopy (FTIR) in a Thermo Nicolet nexus equipped with a Goldengate attenuated total reflectance device. The textural properties of the materials were determined by nitrogen sorption porosimetry by using a Micromeritics ASAP 2020. To perform the N₂ measurements, the samples were previously degassed under vacuum for 24 h at room temperature. Thermogravimetry analysis (TGA) were performed in a Perkin Elmer Pyris Diamond TG/DTA analyzer, with 5 °C min⁻¹ heating ramps, from room temperature to 600 °C. The hydrodynamic size of mesoporous and oleic acid iron oxide nanoparticles were measured by means of a Zetasizer Nano ZS (Malvern Instruments) equipped with a 633 nm "red" laser. Transmission electron microscopy (TEM) was carried out with a JEOL JEM 2100 instruments operated at 200 kV, equipped with a CCD camera (KeenView Camera). Sample preparation was performed by dispersing in distilled water and subsequent deposition onto carbon-coated copper grids. A solution of 1% of phosphotungstic acid (PTA) pH 7.0 was employed as staining agent in order to visualize the polymer coating attached on the mesoporous surface. Scanning electron microscopy (SEM) analyses were made on a JEOL 7600-LINK AN10000 microscope (Electron Microscopy Centre, UCM) using a graphite sample holder without any treatment. Liquid ¹H-NMR experiments were made in a Bruker AV 250MHz. UV-Vis spectrometry was used to determine the LCST of linear polymers by means of a Biotek Synergy 4 device. Iron quantification for specific absorption rate (SAR) measurements at 480 nm absorbance was carried out on a Thermo Scientific Multiskan GO UV/Vis microplate spectrophotometer. A calibration curve was performed following the same procedure using iron standard solution (Acros Organics) as reference. DC magnetic field: magnetic parameters were determined by means of a vibrating sample magnetometer (VSM, Instituto de Sistemas Optoelectrónicos y Microtecnología, Universidad Politécnica de Madrid, Spain). Measurements were carried out at room temperature and applying a maximum DC field of 5000G. The AMF assays were performed on a DM100 system (nanoScale Biomagnetics) in the frequency range from 424 kHz to 838 kHz and magnetic fields of 20.05 to 23.87 kA·m⁻¹.

Calculation Procedures : The surface area was determined using the Brunauer-Emmett-Teller (BET) method and the pore volume, V_{pore} (cm³ g⁻¹), was estimated from the amount of N₂ adsorbed at a relative pressure around 0.99. The pore size distribution between 0.5 nm and 40 nm was calculated from the desorption branch of the

1 isotherm by means of the Barrett-Joyner-Halenda (BJH) 8
2 method. The mesopore size, ϕ_{pore} (nm), was determined 5 9
3 from the maximum of the pore size distribution curve 6 0
4 The SAR calculations were performed by DM100 system 6 1
5 software (nanoScale Biomagnetics). The mole percentage 6 2
6 of NHMA (f_{NHMA}) in the synthesized random copolymer 6 3
7 was determined using ^1H NMR analysis using equation 1.6 4
8 $I_{4.66 \text{ ppm}}$ and $I_{3.87 \text{ ppm}}$ are the integrals of the protons at 4.66 5
9 ppm and 3.87 ppm respectively. 6 6

$$10 f_{\text{NHMA}}(\%) = \frac{I_{4.66 \text{ ppm}/2}}{I_{3.87 \text{ ppm}} + I_{4.66 \text{ ppm}/2}} \times 100 \quad (i) \quad 6 7$$

11 **Preparation of Hydrophobic Magnetite (Fe_3O_4)** 7 0
12 **NPs.** Hydrophobic magnetite NPs were synthesized by 7 1
13 one-pot chemical coprecipitation method. Deionized 7 2
14 water was purged with nitrogen gas for 10 min. Then, 4.8 7 3
15 g of $\text{FeCl}_3 \cdot 6\text{H}_2\text{O}$, 2.00 g $\text{FeCl}_2 \cdot 4\text{H}_2\text{O}$, and 0.85 mL oleic 7 4
16 acid were added to 30 mL of deionized water under nitro 7 5
17 gen atmosphere with vigorous stirring. The mixture solu 7 6
18 tion was heated to 90 °C. Then, 20 mL of ammonium 7 7
19 hydroxide (14 wt %) was added rapidly to the solution 7 8
20 and it immediately turned black. The reaction was kept at 7 9
21 90 °C for 2.5 h and then allowed to cool to room tempera 8 0
22 ture. The black precipitate was collected by magnetic 8 1
23 decantation and resuspended in chloroform with an end 8 2
24 concentration of 32.8 mg·mL⁻¹ oleic acid-capped Fe_3O_4 . 8 3

25 **Preparation of Mesoporous Magnetic Silica Nano-** 8 4
26 **particles (MMSNPs).** MMSNPs were prepared in a 50 mL 8 5
27 round-bottom flask, adding 582 mg of CTAB as a phase 8 6
28 transfer agent and structure-directing agent for silica 8 7
29 condensation that were dissolved in 10 mL of H_2O (mQ) 8 8
30 Then, the mixture was mechanically stirred in an ultra 8 9
31 sound bath during the addition of 26.4 mg OA- Fe_3O_4 (9 0
32 CHCl_3 , 0.04 mL·min⁻¹ rate) until the complete removal of 9 1
33 the organic solvent. The aqueous suspension was added 9 2
34 through a 0.2 μm cellulose filter to an 86 mL NaOH 9 3
35 (0.016M) solution and stirred at 600rpm. When the sus- 9 4
36 pension was stabilized at 45 °C, a mixture of 1.2 mL 9 5
37 EtOH and 1 mL of TEOS was added dropwise (0.2 9 6
38 mL·min⁻¹ rate). Once the TEOS addition was finished 9 7
39 130 μL of PEG-Si were added, and the suspension was 9 8
40 stirred for 2h. The reaction mixture was washed three 9 9
41 times by centrifugation with 50 mL of H_2O , and then tw 10 0
42 ore times with 50 mL of EtOH. The brown solid ob 10 1
43 tained was suspended in 200 mL of EtOH (99.5%). Then 10 2
44 0.5 mL of MPS were added dropwise and the mix was kept 10 3
45 stirring at 40 °C during 16h. Before the washing step with 10 4
46 absolute EtOH, the surfactant template was removed by 10 5
47 ion exchange using 175mL of 10 g·L⁻¹ NH_4NO_3 in EtOH 10 6
48 (95%) extracting solution at 65°C overnight. The brown 10 7
49 suspension was then centrifuged (15000 rpm, 30 min) and 10 8
50 washed three times with 50 mL of EtOH to be dried under 10 9
51 vacuum overnight. 11 0

52 **Linear Polymers Synthesis.** In a typical synthesis for a 11 1
53 polymer with a 90:10 NIPAM to NHMA ratio, 200mg (1.76 11 2
54 mmol) of NIPAM and 44.8 μL (0.19 mmol) of NHMA were 11 3
55 placed in vial A and 12.7 mg of initiator 4,4'-Azobis(41 14
56 cyanovaleric acid) (ABCVA) were placed in vial B. The 11 5
57 monomer mixture and the initiator were purged by nitro 11 6

gen flow prior to the addition of 2.5 mL and 1 mL of dry 11 8
DMF respectively to each vial. The solutions were bubb 11 9
led with N_2 for 15 min. Vial A was stirred in a heated 12 0
oilbath at 80 °C for 2 min before the fast addition of 100 μL 12 1
of vial B solution (1.2 mg, 400:1 monomer to initiator ra 12 2
tio) and allowed to stir for 16 h. A maximum 2mL of the 12 3
reaction mixture were added dropwise to 45 mL of EtO₂ 12 4
in a centrifugation tube obtaining a white precipitate. The 12 5
precipitate was washed three times with 45 mL of diethy 12 6
lether and dried at ambient temperature. The white solid 12 7
was dissolved in H_2O and lyophilized. 12 8

MMSNPs Polymer Coating. In a 100 mL three-neck 13 0
round-bottom flask, 150.9 mg (1.33 mmol) of NIPAM, 12 1
mg of MBA (0.078mmol), 49.4 μL of NHMA (0.148 mmol), 13 2
3.6 mg of CTAB and 5 mg of Na_2CO_3 were added to 45 mL 13 3
of water (mQ). The solution was stirred under N_2 bub 13 4
bling at 70 °C for 30 min to remove oxygen. Then, the 13 5
solution was kept under N_2 and 50 mg of MMSNPs redis 13 6
persed in 5 mL of EtOH (99.5%) were added to the mon 13 7
omer solution and stirred for 15 min more. To initiate the 13 8
monomer polymerization 0.2 mL of a 25 mg·mL⁻¹ APS 13 9
solution in H_2O (mQ) previously deoxygenated were 14 0
added to the reaction mixture. 20 min before the initiator 14 1
addition appears a brown solid precipitate and the reac 14 2
tion mixture was allowed to cool down to room tempera 14 3
ture and kept at that temperature for 6 h. The mixture 14 4
was centrifuged and washed three times with H_2O to 14 5
remove the unreacted monomers and be dried under 14 6
vacuum overnight. 14 7

Fluorescein Release Experiments. Hybrid 15 0
MMSN@P(NIPAM/NHMA) nanoparticles were loaded 15 1
with a 20 mg·mL⁻¹ fluorescein sodium salt solution in PBS 15 2
(1x) at 50 °C for 16 h. Then, the hybrid material was 15 3
washed with PBS (1x) until no fluorescence was observed. 15 4
Fluorescein release experiments were carried out with 10 15 5
mg of fluorescein loaded MMSN@P(NIPAM/NHMA) 15 6
dispersed in 1 mL of PBS (1x) and divided in two 0.5 mL 15 7
aliquots. To determine the polymer VPTT attached to the 15 8
silica surface one aliquot was submitted to a heating ramp 15 9
in an incubator to the three target temperatures (37 °C, 40 16 0
°C and 43 °C). The second aliquot was carried to AC mag 16 1
netic inductor to apply an 838 KHz and 20.05 kA·m⁻¹ al 16 2
ternating magnetic field. The temperature increase devel 16 3
oped by the nanoparticles was recorded with a fiber-optic 16 4
probe. After the dispersion reached the target tempera 16 5
ture the samples were cooled down, collected by centrifu 16 6
gation and the fluorescence of supernatants was meas 16 7
ured. Isotherm fluorescein release experiment was made 16 8
keeping one of the aliquots placed in the AC magnetic 16 9
inductor under isotherm conditions at 37°C with a water 17 0
recirculating system. The other aliquot was kept at 37 °C 17 1
in an incubator as control. Alternating magnetic field was 17 2
applied. After 45 min the samples were cooled to 4 °C, 17 3
collected by centrifugation and the fluorescence of super 17 4
natants was measured. 17 5

17 6 RESULTS AND DISCUSSION

17 7 Ultrastable hydrophobic oleic acid iron oxide nanocrys 17 8
tals (OA- Fe_3O_4) were obtained by the co-precipitation 17 9
method previously described by Haynes and colleagues²⁴, 18 0

1 obtaining a colloidal suspension in organic solvent of 0
 2 nanoparticles that present a diameter distribution cen-6 1
 3 tered on 6 nm, confirmed by TEM images (Figure S1).6 2
 4 Then, these magnetic cores were transferred to an aque6 3
 5 ous phase using n-cetyltrimethylammonium bromide6 4
 6 (CTAB) solution, which acts as a phase transfer agent and 5
 7 as porous structure-directing agent at the same time.
 8 Next, a mesoporous silica matrix was formed by the slow
 9 addition of tetraethyl orthosilicate (TEOS) in the pres-
 10 ence of NaOH as a catalyst. After the addition of TEOS, a
 11 solution of silylated poly (ethyleneglycol) (Hy-
 12 droxy(polyethyleneoxy)propyl] tri-ethoxysilane, PEG-Si,
 13 MW = 575-750 g/mol) was incorporated in the reaction
 14 mixture in order to avoid self-aggregation in the reaction
 15 media. Finally, 3-[Tris(trimethylsiloxy)silyl]propyl meth-
 16 acrylate (MPS) was added, to provide polymerizable
 17 groups on the particle surface. Passivation with PEG helps
 18 to maintain the nanoparticle dispersity and long-term
 19 stability in various biological media and phosphate buff-
 20 ered saline (PBS).²⁵ At this point, a distribution of 78 nm
 21 magnetic mesoporous nanoparticles was obtained by
 22 dynamic light scattering that was also confirmed by SEM
 23 and TEM images (Figure S2). The organic content of the
 24 particles was determined by thermogravimetric analysis
 25 (TGA) having a 10% weight loss (Figure S3), correspond-
 26 ing to PEG and methacrylate groups on the silica surface.
 27 This was also confirmed by the FTIR spectra of the materi-
 28 al that exhibited the characteristic ν_{as} (OC=O) ester
 29 band of the methacrylate groups at 1700 cm^{-1} and σ (CH)
 30 at 1472 cm^{-1} from both functionalizing agents (Figure S4).
 31 Textural parameters were evaluated by N_2 porosimetry
 32 showing a profile of mesoporous adsorption-desorption
 33 isotherms and surface area of $1391\text{ m}^2\cdot\text{g}^{-1}$ (Figure S5 and
 34 table S1) which confers high loading capacity for drug
 35 delivery purposes²⁶.
 36 Thermosensitive polymers based on poly-*N*-7 1
 37 isopropylacrylamide (pNIPAm) are widely used for drug
 38 delivery applications because it can undergo a linear to
 39 globular phase transition when heated above its lower
 40 critical solution temperature (LCST), which is $32\text{ }^\circ\text{C}$ ²⁷ and
 41 it presents good biocompatibility.²⁸ The stimuli-
 42 responsive behavior of pNIPAm based polymers arises
 43 from the entropic gain produced when water molecules
 44 attached by hydrogen-bonding to the polymer chains are
 45 discharged to the aqueous phase above the lower critical
 46 solution temperature (LCST) or volume phase transition
 47 temperature (VPTT) when crosslinkers are used. This
 48 entropy change is responsible for the transition from
 49 hydrophilic to hydrophobic state. However, the LCST of
 50 pNIPAm is not suitable for drug delivery applications,
 51 it is below the body temperature. For the purpose of this
 52 work, a thermosensitive polymer with an LCST of $42-48$
 53 $^\circ\text{C}$ was desired, in order to be in its swelling state (and
 54 pore-blocking) at the body temperature ($37\text{ }^\circ\text{C}$) and col-
 55 lapsed (and pore opening) when heated in temperatures
 56 between $42\text{ }^\circ\text{C}$ to $45\text{ }^\circ\text{C}$. Therefore, we introduced hydro-
 57 philic co-monomers in the pNIPAm chain to increase the
 58 polymer transition temperature, specifically *N*-
 59 hydroxymethyl acrylamide (NHMA), which increases the

polymer-water interactions resulting in a LCST or VPTT
 enhancement. In order to synthesize a suitable polymer
 which suffers a polymer transition in the $41\text{ }^\circ\text{C}$ to $43\text{ }^\circ\text{C}$
 temperature range, we first synthesized a library of linear
 polymers by radical polymerization in liquid phase using
 different NIPAM/NHMA monomer ratios (Figure 1).

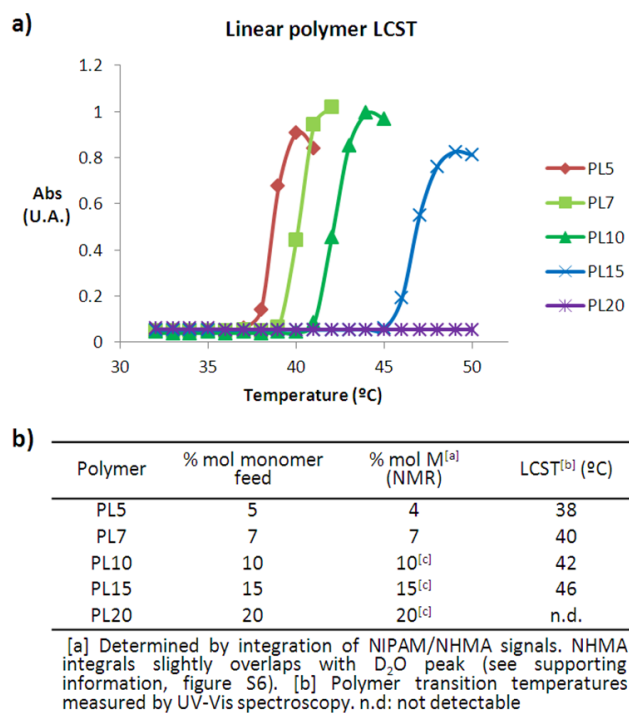
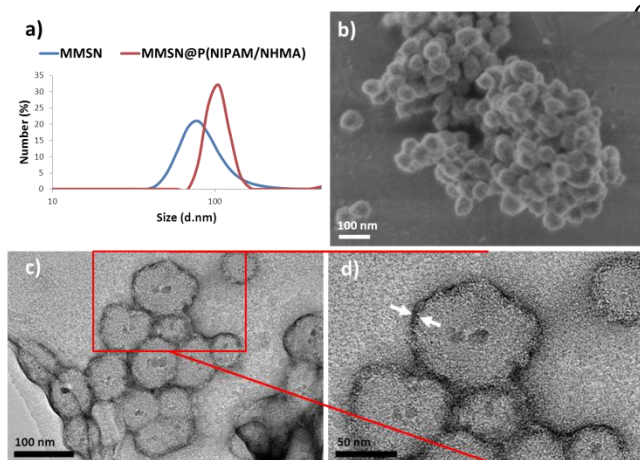


Figure 1. Lower critical solution temperature changes with the increase of hydrophilic monomer NHMA for linear polymers measured by turbidimetry (a) and polymerization data obtained using 1/400 monomer-to-initiator ratio (b).

The transition temperature of the synthesized polymers was determined by UV-VIS spectrometry keeping the pH and the ionic strength fixed at 7.4 and 0.0134 M following a procedure described in the supporting information. As expected, the LCST of the polymers augmented as the hydrophilic monomer ratio increased, while the LCST behavior was not detectable when 20% of monomer was employed. Once we screened our prepared co-polymers library, we chose for further *in situ* polymer attachment, a feed monomer ratio of 90:10 NIPAM/NHMA, which resulted in a polymer with and LCST of $42\text{ }^\circ\text{C}$. Polymeric layer was carried out by a slight modification of the method developed by Yang *et al*²⁹. Therefore, this NIPAM/NHMA ratio was used to coat the MMSNPs, in the presence of methylene bisacrylamide (MBA) for cross-linking purposes. After the polymeric shell incorporation, the MMSNPs average size distribution raised from 78nm to 100nm as measured by dynamic light scattering and in accordance with SEM and TEM images. Besides, the mesoporous structure was retained and the polymeric coating became clearly visible upon staining the nanoparticles with uranyl acetate (UA) and TEM observation following a similar method reported elsewhere³⁰ (Figure 2). The amount of grafted polymer was 26 % as determined by TGA (Figure S3) and FTIR demonstrated a characteristic

1 ν_{as} (NC=O) amide band at 1650 cm^{-1} showing the grafting
 2 of the polymeric shell (Figure S4). Stability studies carried
 3 out in PBS by DLS demonstrated that the colloidal sus-
 4 pension was maintained for 8 h, thanks to the polymeric
 5 coating (Figure S7).

6 In order to assess the magnetically responsive behavior,
 7 the polymer coated mesoporous nanoparticles were char-
 8 acterized under DC (direct current) and AC (alternating
 9 current) magnetic field conditions. DC experiments
 10 showed loops with coercive fields close to zero and satu-
 11 ration magnetization values of $2.80\text{ emu}\cdot\text{g}^{-1}$, evidencing
 12 the superparamagnetic behavior of the SPIONS contained
 13 within the silica matrix (Figure S8). Different conditions
 14 were considered for AC experiments using different fre-
 15 quencies and field amplitudes listed in table S2. A maxi-
 16 mum SAR of $178.53\text{ W}\cdot\text{g}^{-1}$ was registered for AC fields of
 17 $20.05\text{ kA}\cdot\text{m}^{-1}$ and 838 kHz . Therefore these AC field pa-
 18 rameters were selected for further experiments.

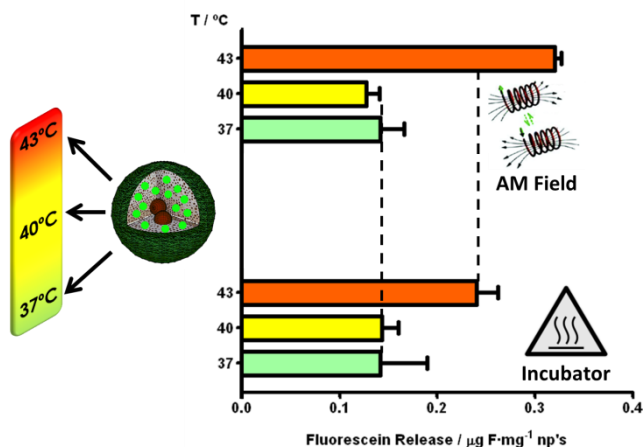


19 **Figure 2.** DLS measurements of MMSNPs and
 20 MMSN@P(NIPAM/NHMA) (a). SEM micrographs (b) and
 21 TEM images (c) of the polymer coated nanoparticles. Poly-
 22 meric coating detail (d).

23 The addition of MBA as a cross-linker to obtain a dense
 24 polymer network, besides the surface coating process,
 25 could affect the polymer transition temperature of the
 26 nanodevice. Additionally, the attachment of a polymer
 27 onto a nanoparticle could also affect its temperature-
 28 responsive behavior. However, LCST measurements in
 29 the presence of MMSN@P(NIPAM/NHMA) were not possible, due to the UV
 30 light scattering of the nanoparticles. In order to confirm
 31 that the transition temperature of the polymer coating is
 32 maintained after immobilization on the surface, a colloidal
 33 suspension of 10 mg/mL fluorescein loaded
 34 MMSN@P(NIPAM/NHMA) nanoparticles were placed in
 35 an incubator. The target temperatures were chosen to be
 36 $37\text{ }^{\circ}\text{C}$, $40\text{ }^{\circ}\text{C}$ and $43\text{ }^{\circ}\text{C}$. After reaching the target temperatures
 37 the samples were collected and the fluorescence of the
 38 supernatants (released fluorescein) was measured. The
 39 amounts of released fluorophore were similar at $37\text{ }^{\circ}\text{C}$ and
 40 $40\text{ }^{\circ}\text{C}$, but once the global temperature reached $43\text{ }^{\circ}\text{C}$, an
 41 increase in fluorescein release was clearly observed (Fig-
 42 ure 3). This fact indicates that the thermosensible poly-
 43 mer coating has its VPTT near LCST linear polymer be-

45 havior and transition temperature, being able to retain its
 46 cargo at physiological temperature and release it once the
 47 temperature overcomes the VPTT value, even with a high-
 48 ly-soluble model drug as the fluorescein sodium salt.
 49 Time evolution of the fluorescein release was also tested
 50 at $37\text{ }^{\circ}\text{C}$ and $50\text{ }^{\circ}\text{C}$, showing a low premature release of $20\text{ }\%$
 51 of the cargo within the first 24 h (Figure S9). This result
 52 indicates that this device would release the most of its
 53 cargo once the target tissue was reached and AMF will be
 54 applied.

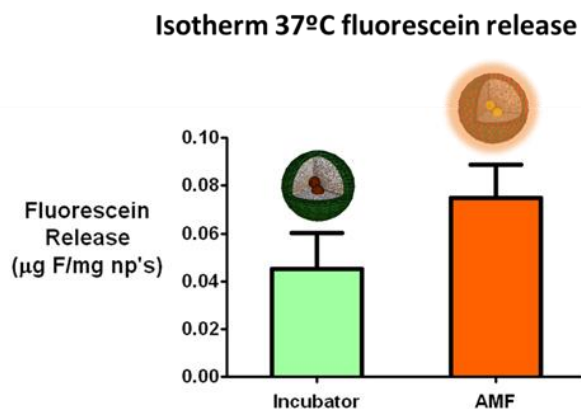
55 Therefore, the same experiment was repeated by expos-
 56 ing the fluorescein loaded particles to an AMF at a fre-
 57 quency of 838 kHz and a field of $20.05\text{ kA}\cdot\text{m}^{-1}$. The tem-
 58 perature was monitored using a fiberoptic temperature
 59 probe and the temperature ramp was replicated to three
 60 different global temperatures of $37\text{ }^{\circ}\text{C}$, $40\text{ }^{\circ}\text{C}$ and $43\text{ }^{\circ}\text{C}$
 61 similarly to that obtained with the incubator (Figure S10).
 62 The samples submitted to an AMF presented a similar
 63 fluorescein release profile at the three target temperatures
 64 (Figure 3).



65 **Figure 3.** Fluorescein release of polymer coated nanoparti-
 66 cles at different target temperatures in an incubator (below)
 67 and under AMF application (above).

68 Below the polymer's VPTT, the fluorescein release was
 69 low compared to the sample that reached $43\text{ }^{\circ}\text{C}$, revealing
 70 that it is possible to provoke the polymer transition under
 71 an alternating magnetic field, as we have previously de-
 72 scribed¹³. Moreover, there was a significant difference in
 73 the released cargo between the samples exposed to ther-
 74 mal and magnetic heating after reaching the VPTT. As it
 75 is clearly shown in figure 3, the sample exposed to mag-
 76 netic field was able to release a significantly higher
 77 amount of fluorescein in the same period of time. This
 78 variance in fluorescein release could be explained by dif-
 79 ferent mechanisms: (i) the polymer transition tempera-
 80 ture is reached faster in the particle surroundings when
 81 AMF is applied, which is consistent with previously cited
 82 works,^{18,19} (ii) the localized temperature at the nanoparti-
 83 cle proximities is higher than the global temperature,
 84 which causes a faster diffusion of the loaded molecules
 85 once the pore is opened and (iii) the vibrations of the
 86 SPIONS when subjected to AMF can also induce a higher
 87 release as compared to simple heating in the incubator.

1 These mechanisms could act cooperatively resulting in
 2 the enhanced fluorescein release.
 3 The response to heat dissipation by physiological envi-
 4 ronment is a critical issue still unclear. There are doubts
 5 whether these magnetic devices are capable to overcome
 6 the heat dissipation that is observed in living tissues. To
 7 resolve this matter of concern, we developed a second
 8 experiment by applying AMF under isotherm conditions,
 9 keeping constant the temperature at 37°C with a water
 10 recirculating system while the AMF is applied. Then, the
 11 fluorescein release experiment was performed using this
 12 isothermal set-up, placing one aliquot in the AC magnetic
 13 inductor at 37°C, while another aliquot was placed at 37
 14 °C in an incubator as control. The alternating magnetic
 15 field was applied for 45 min. Subsequently, the samples
 16 were rapidly cooled to 4 °C to avoid fluorescein leaking,
 17 collected by centrifugation and the fluorescence of super-
 18 natants was measured. Results showed a 2-fold fluorescein
 19 release upon an AMF application with regard to the
 20 sample placed in an incubator (Figure 4).



21
 22 **Figure 4.** Fluorescein release from
 23 MMSN@P(NIPAM/NHMA) under AMF in isothermal con-
 24 ditions.

25 CONCLUSIONS

26 This fact proves that thermal energy dissipated by SPI-
 27 ONs under a magnetic field is capable to effectively reach
 28 the surface of the nanoparticles through the silica matrix,
 29 provoking the polymer hydrophilic to hydrophobic transi-
 30 tion and the subsequent drug release when under iso-
 31 thermal conditions at 37°C, which mimics the physiologi-
 32 cal conditions. This phenomenon can be explained by the
 33 so called *hot spot* effect, where the existence of a hot
 34 source in the interior of the device accomplishes high
 35 local temperatures but no global heating is observed.

36 This work shows that the application of an AMF to our
 37 system provokes the release of the cargo without the
 38 necessity to achieve a global temperature increase. The
 39 hot spots generated by magnetite nanoparticles are capa-
 40 ble to provoke the shrinkage of the polymer network on
 41 the silica matrix, achieving the effective triggered release
 42 of the cargo. It must be highlighted that the aim of this
 43 work is not demonstrating the hot spot effect, but its
 44 capability for releasing the cargo in a stimuli-responsive

way, although the environment remained at physiological
 temperature. Heating the environment requires much
 magnetic energy that, very often, is non-compatible with
 the clinical/technical requirements, which is a very seri-
 ous limitation for the transference to the biomedical
 field.³¹ These results pave the way to the application of
 magnetically triggered carriers for the treatment of com-
 plex diseases due to the biocompatibility and high pen-
 etration capacity of magnetic fields. Moreover, the pres-
 ence of magnetic cores within the silica matrix opens the
 possibility to combine the stimuli-responsive capacity
 with imaging applications in the same carrier, converting
 this device in an excellent prototype in the theranostics
 field. Further work is ongoing in order to test the capacity
 of this device to transport and release cytotoxic drugs
 using *in vivo* models.

61 ASSOCIATED CONTENT

62 **Supporting Information.** Characterization techniques as
 63 transmission and scanning electron microscopy, dynamic
 64 light scattering, nitrogen sorption isotherms, IR and NMR
 65 spectroscopy, release experiments, thermogravimetric ana-
 66 lysis, vibrating sample magnetometer and SAR measure-
 67 ments, Figures S1–S10 and Tables S1 and S2 are showed in this
 68 associated content, as well as materials and methods used for
 69 the preparation of the nanoparticles. This material is availa-
 70 ble free of charge via the Internet at <http://pubs.acs.org>.

1 AUTHOR INFORMATION

2 Corresponding Author

*E-mail: vallet@ucm.es, Phone 34 91 3941870. Fax 34 91
 4 3941786.

Author Contributions

The manuscript was written through contributions of all
 authors. All authors have given approval to the final version
 of the manuscript.

79 ACKNOWLEDGMENT

80 This work was supported by the Ministerio de Economía y
 81 Competitividad, through projects MAT2012-35556, MAT2013-
 82 43299R and CSO2010-11384-E (Ageing Network of Excel-
 83 lence), ERC-Starting Grant 239931-NANOPUZZLE project,
 84 Fondo Social Europeo (FSE; Gobierno de Aragón), CIBER-
 85 BBN is an initiative funded by the VI National R&D&i Plan
 86 2008-2011, Iniciativa Ingenio 2010, Consolider Program,
 87 CIBER Actions and financed by the Instituto de Salud Carlos
 88 III with assistance from the European Regional Development
 89 Fund.. We also thank the X-ray Diffraction C.A.I., NMR
 90 C.A.I. and the National Electron Microscopy Center, UCM. E.
 G. thanks CEI Campus Moncloa for the PICATA fellowship.

92 REFERENCES

- (1) Jain, R. K.; Stylianopoulos, T. Delivering Nanomedicine to Solid Tumors. *Nat. Rev. Clin. Oncol.* **2010**, *7*, 653–664.
- (2) Baeza, A.; Colilla, M.; Vallet-Regí, M. Advances in Mesoporous Silica Nanoparticles for Targeted Stimuli-Responsive Drug Delivery. *Expert Opin. Drug Deliv.* **2015**, *12*, 319–337.

- 1 (3) Vallet-Regí, M.; Rámila, a.; Del Real, R. P.; Pérez-Pariente, J. 5 4 (16) Wust, P.; Hildebrandt, B.; Sreenivasa, G.; Rau, B.;
2 A New Property of MCM-41: Drug Delivery System. *Chem.* 5 5 Gellermann, J.; Riess, H.; Felix, R.; Schlag, P. M.
3 *Mater.* **2001**, *13*, 308–311. 5 6 Hyperthermia in Combined Treatment of Cancer. *Lancet*
5 7 *Oncol.* **2002**, *3*, 487–497.
- 4 (4) Maeda, H.; Nakamura, H.; Fang, J. The EPR Effect for 5 8 (17) Dutz, S.; Hergt, R. Magnetic Nanoparticle Heating and
5 Macromolecular Drug Delivery to Solid Tumors: 5 9 Heat Transfer on a Microscale: Basic Principles, Realities
6 Improvement of Tumor Uptake, Lowering of Systemic 6 0 and Physical Limitations of Hyperthermia for Tumour
7 Toxicity, and Distinct Tumor Imaging in Vivo. *Adv. Drug 6 1 Therapy.* *Int. J. Hyperthermia* **2013**, *29*, 790–800.
- 8
9 (5) Wicki, A.; Witzigmann, D.; Balasubramanian, V.; Huwyler, 6 2 (18) Dias, J. T.; Moros, M.; Del Pino, P.; Rivera, S.; Grauz, V.; de
10 J. Nanomedicine in Cancer Therapy: Challenges, 6 3 la Fuente, J. M. DNA as a Molecular Local Thermal Probe
11 Opportunities, and Clinical Applications. *J. Control. Release* 6 4 for the Analysis of Magnetic Hyperthermia. *Angew. Chem.*
12 **2015**, *200*, 138–157. 6 5 *Int. Ed. Engl.* **2013**, *52*, 11526–11529.
- 13 (6) Angelos, S.; Khashab, N. M.; Yang, Y. W.; Trabolsi, A.; 6 6 (19) Riedinger, A.; Guardia, P.; Curcio, A.; Garcia, M. A.;
14 Khatib, H. a.; Stoddart, J. F.; Zink, J. I. pH Clock-Operated 6 7 Cingolani, R.; Manna, L.; Pellegrino, T. Subnanometer Local
15 Mechanized Nanoparticles. *J. Am. Chem. Soc.* **2009**, *131*, 6 8 Temperature Probing and Remotely Controlled Drug
16 12912–12914. 6 9 Release Based on Azo-Functionalized Iron Oxide
7 0 Nanoparticles. *Nano Lett.* **2013**, *13*, 2399–2406.
- 17 (7) Chen, L.; Li, L.; Zhang, L.; Xing, S.; Wang, T.; Wang, Y. A.; 7 1 (20) Dong, J.; Zink, J. I. Taking the Temperature of the Interiors
18 Wang, C.; Su, Z. Designed Fabrication of Unique Eccentric 7 2 of Magnetically Heated Nanoparticles. *ACS Nano* **2014**, *8*,
19 Mesoporous Silica Nanocluster-Based Core-Shell 7 3 5199–5207.
20 Nanostructures for pH-Responsive Drug Delivery. *ACS*
21 *Appl. Mater. Interfaces* **2013**, *5*, 7282–7290.
- 22 (8) Mackowiak, S. A.; Schmidt, A.; Weiss, V.; Argyo, C.; Von, C. 7 4 (21) Kim, J.; Kim, H. S.; Lee, N.; Kim, T.; Yu, T.; Song, I. C.;
23 Targeted Drug Delivery in Cancer Cells with Red Light 7 5 Moon, W. K.; Hyeon, T. Multifunctional Uniform
24 Photoactivated Mesoporous Silica Nanoparticles. *Nano 7 6 Nanoparticles Composed of a Magnetite Nanocrystal Core*
25 *Let.* **2013**, *13*, 1–19. 7 7 and a Mesoporous Silica Shell for Magnetic Resonance and
7 8 Fluorescence Imaging and for Drug Delivery. *Angew.*
7 9 *Chemie* **2008**, *120*, 8566–8569.
- 26 (9) Zhang, J.; Yuan, Z. F.; Wang, Y.; Chen, W. H.; Luo, G. F.; 8 0 (22) Lin, Y.-S.; Hurley, K. R.; Haynes, C. L. Critical
27 Cheng, S. X.; Zhuo, R. X.; Zhang, X. Z. Multifunctional 8 1 Considerations in the Biomedical Use of Mesoporous Silica
28 Envelope-Type Mesoporous Silica Nanoparticles for Tumor 8 2 Nanoparticles. *J. Phys. Chem. Lett.* **2012**, *3*, 364–374.
29 Triggered Targeting Drug Delivery. *J. Am. Chem. Soc.* **2013**, 8 2
30 *135*, 5068–5073.
- 31 (10) Slowing, I. I.; Trewyn, B. G.; Giri, S.; Lin, V. S. Y. 8 3 (23) Meng, H.; Xue, M.; Xia, T.; Ji, Z.; Tarn, D. Y.; Zink, J. I.; Nel,
32 Mesoporous Silica Nanoparticles for Drug Delivery and 8 4 A. E. Use of Size and a Copolymer Design Feature to
33 Biosensing Applications. *Adv. Funct. Mater.* **2007**, *17*, 1225–8 6 Improve the Biodistribution and the Enhanced
34 1236. 8 7 Permeability and Retention Effect of Doxorubicin-Loaded
8 8 Mesoporous Silica Nanoparticles in a Murine Xenograft
Tumor Model. *ACS Nano* **2011**, *5*, 4131–4144.
- 35 (11) Tarn, D.; Ashley, C. E.; Xue, M.; Carnes, E. C.; Zink, J. I.; 8 9 (24) Lin, Y.-S. S.; Haynes, C. L. Synthesis and Characterization of
36 Brinker, C. J. Mesoporous Silica Nanoparticle Nanocarriers 8 9 Biocompatible and Size-Tunable Multifunctional Porous
37 Biofunctionality and Biocompatibility. *Acc. Chem. Res.* 9 0 Silica Nanoparticles. *Chem. Mater.* **2009**, *21*, 3979–3986.
38 **2013**, *46*, 792–801. 9 1
- 39 (12) Ruiz-Hernández, E.; Baeza, A.; Vallet-Regí, M. Smart Drug 9 2 (25) Lin, Y.-S.; Abadeer, N.; Haynes, C. L. Stability of Small
40 Delivery through DNA/Magnetic Nanoparticle Gates. *ACS* 9 3 Mesoporous Silica Nanoparticles in Biological Media.
41 *Nano* **2011**, *5*, 1259–1266. 9 4 *Chem. Commun.* **2011**, *47*, 532–534.
- 42 (13) Baeza, A.; Guisasaola, E.; Ruiz-Hernández, E.; Vallet-Regí, M. 9 5 (26) Vallet-Regí, M.; Balas, F.; Arcos, D. Mesoporous Materials
43 Magnetically Triggered Multidrug Release by Hybrid 9 6 for Drug Delivery. *Angew. Chemie - Int. Ed.* **2007**, *46*, 7548–
44 Mesoporous Silica Nanoparticles. *Chem. Mater.* **2012**, *24*, 9 7 7558.
45 517–524.
- 46 (14) Chang, B.; Sha, X.; Guo, J.; Jiao, Y.; Wang, C.; Yang, W. 9 8 (27) Schild, H. G. Poly (N-Isopropylacrylamide): Experiment ,
47 Thermo and pH Dual Responsive, Polymer Shell Coated, 9 9 Theory and Application. *Prog. Polym. Sci.* **1992**, *17*, 163–249.
48 Magnetic Mesoporous Silica Nanoparticles for Controlled 10 0 (28) Wadajkar, A. S.; Koppolu, B.; Rahimi, M.; Nguyen, K. T.
49 Drug Release. *J. Mater. Chem.* **2011**, *21*, 9239. 10 1 Cytotoxic Evaluation of N-Isopropylacrylamide Monomers
10 2 and Temperature-Sensitive poly(N-Isopropylacrylamide)
10 3 Nanoparticles. *J. Nanoparticle Res.* **2009**, *11*, 1375–1382.
- 50 (15) Liu, C.; Guo, J.; Yang, W.; Hu, J.; Wang, C.; Fu, S. Magnetic 10 3 (29) Chang, B.; Chen, D.; Wang, Y.; Chen, Y.; Jiao, Y.; Sha, X.;
51 Mesoporous Silica Microspheres with Thermo-Sensitive 10 4 Yang, W. Bioresponsive Controlled Drug Release Based on
52 Polymer Shell for Controlled Drug Release. *J. Mater. Chem.* 10 4
53 **2009**, *19*, 4764. 10 5

1	Mesoporous Silica Nanoparticles Coated with Reductively	8	(31)	Brezovich, I. A.; Meredith, R. F. Practical Aspects of
2	Sheddable Polymer Shell. <i>Chem. Mater.</i> 2013 , <i>25</i> , 574–585.	9		Ferromagnetic Thermoseed Hyperthermia. <i>Radiol. Clin.</i>
		10		<i>North Am.</i> 1989 , <i>27</i> , 589–602.
3	(30) Baeza, A.; Guisasola, E.; Torres-Pardo, A.; González-Calbet,			
4	J. M.; Melen, G. J.; Ramirez, M.; Vallet-Regí, M. Hybrid	11		
5	Enzyme-Polymeric Capsules/mesoporous Silica Nanodevice			
6	for in Situ Cytotoxic Agent Generation. <i>Adv. Funct. Mater.</i>	12		
7	2014 , <i>24</i> , 4625–4633.			

SYNOPSIS TOC The key of magnetic triggered stimuli responsive devices is to generate enough thermal energy to trigger the drug release. We proved for the first time the possibility to produce enough local heat to trigger the cargo release without the need of increasing the global temperature in a stimuli-responsive device. This verifies that the so called “hot spot” effect can overcome heat dissipation at physiological temperature.

